Kuwait J.Sci., Vol.49, No.(2),April.2022,pp(1-16)

Numerical modelling of non-premixed biogas and LPG combustion to study carbon nanostructures formation in flame

Manpreet Kaur[1], Jyoti Bharj[1,*], Rabinder S. Bharj[2], Rajan Kumar[2]

[1]*Dept. of Physics, Dr. B.R. Ambedkar National Institute of Technology, Jalandhar, Punjab, India*
[2]*Dept. of Mechanical Engineering, Dr. B.R. Ambedkar National Institute of Technology, Jalandhar, Punjab, India*

**Corresponding author: jyoti@nitj.ac.in*

Abstract

This work presents the numerical simulation of biogas and LPG fuelled diffusion flames in an axisymmetric chamber to study the formation mechanism of soot and carbon nanostructures in these flames. The simulation is formulated on transport equations that involve conservation of mass (the continuity equation), momentum (Navier-Stokes equation), energy, and chemical species. The governing equations are solved using ANSYS FLUENT, centred on the finite volume method. To predict the soot formation, one step soot model has been incorporated. The solution of these equations permits the estimation of the temperature field and species concentrations inside the flame. Simulation is conducted at fixed fuel flow rates and varied oxygen flow rates. The results reveal that the formation of soot and carbon nanostructures is strongly dependent on peak flame temperature and the concentration of precursor species formed in the flame. Since two fuels produce an exclusive chemical environment in the flame, the flame temperature and CO concentration conducive to the growth of carbon nanostructures is higher for LPG fuel than for biogas. Hence, the nucleation process of carbon nanostructures is faster for LPG than biogas. Moreover, the reactions inside the flame at different locations can also be predicted from flame temperature and species concentration at that location. First, pyrolysis of fuel occurs near the burner exit, followed by the nucleation and surface growth of carbon nanostructures in the nearby region and oxidation of formed carbon nanostructures near the flame tip.

Keywords: Combustion; computational fluid dynamics; diffusion; flame; nucleation.

1. Introduction

Carbon nanostructures (CNSs) offer an exciting area of scientific exploration along with a wide range of novel engineering applications that includes sensors, photovoltaics, field emission transistors, fuel cells, supercapacitors, biomaterials, *etc.* (Kurzepa *et al.*, 2014; Wang *et al.*, 2015). However, these are generally procured under severe conditions ($T > 5000°C$) using arc discharge or laser, plasma ablation, leading to high production costs. Researchers have therefore introduced an alternative method that is relatively cost-effective and energy-efficient. It involves using a hydrocarbon flame to procure these structures (Vander Wal *et al.*, 2000; Yuan *et al.*, 2003). The soot produced in the flame is collected on different substrates to grow a variety of nanostructures from it.

However, the burner flame becomes highly complex due to mass, momentum, and energy transfer in a turbulent flow regime. Simulation tools often serve in understanding the chemistry of complicated phenomena (Mahdavian, 2017). The detailed fluid flow dynamics and flame parameters like optimal fuel to air ratio, the temperature distribution in the core of the flame, and concentration of reactants and products in the flame can be easily obtained using advanced computational fluid dynamic (CFD) tools (Noor *et al.*, 2013; Patel and Shah, 2017; Zohra *et al.*, 2017).

Various theoretical researchers have studied other flame systems to form soot using different turbulent chemistry models. Kaplan and Kailasanath (2001) have simulated normal and inverse non-premixed flames to examine the influence of fuel to air velocity ratio on soot formation in these flames. The results indicate that the regular and inverse diffusion flames have different sooting characteristics. The total quantity of soot produced with normal flame is relatively higher than that generated with inverse flame at the same fuel and air velocities values. However, the volume fraction of soot among three normal flames increases with an increase in fuel-to-air velocity ratio. Smooke *et al.* (2005) have studied the soot formation in laminar co-flow diffusion flame in terms of fuel dilution by inert nitrogen. The results indicate that the peak soot volume fraction increases with an increase in ethylene fuel content, and the peak in surface growth tends to migrate away from the central line towards the wings of the flame with an increase in fuel fraction. Soot formation in turbulent C_2H_4-air diffusion flame using two different turbulent-chemistry interaction models (steady laminar flamelet and flamelet-generated manifold) has been studied by Busupally and De (2016) and has found that both models precisely anticipate the flame length and soot-turbulence interactions.

The present work intends to perform the numerical analysis of biogas and LPG fuelled diffusion flames to study the flame environment in each case, which significantly impacts soot and carbon nanostructures formation. Experiments have already been conducted with these fuels (Singh *et al.,* 2012; Bharj *et al.,* 2014). However, the numerical investigation helps in understanding flow dynamics inside the flame. It can thus help predict the optimum flame parameters that can lead to significant soot and carbon nanostructures growth for future experiments. ANSYS Fluent software based on the finite volume method is used to conduct the numerical analysis (Choudhary *et al.*, 2015).

2. Mathematical formulation

The generalized transport equations that govern mass conservation (the continuity equation), momentum conservation (Navier-Stokes equation), energy and species conservation (Shirneshan and Jamalvand, 2016) are,

2.1 Mass conservation

For steady-state conditions, the continuity equation can be expressed as,

$$\nabla.(\rho \boldsymbol{u}) = 0 \tag{1}$$

Where u is the velocity and ρ is the density of the gaseous mixture.

2.2 Momentum conservation

The fluid flow equation is given by,

$$\rho \frac{D\boldsymbol{u}}{Dt} = -\nabla p + \mu \nabla^2 \mathbf{u} + \rho \boldsymbol{F} \tag{2}$$

Where p is the pressure, μ is the dynamic viscosity of the gaseous mixture, and $\boldsymbol{F}$ is the resultant of volume forces per unit mass of fluid, respectively.

2.3 Energy conservation

The internal energy balance for fluid can be written as,

$$\frac{D\boldsymbol{E}}{Dt} = -\frac{p\Delta}{\rho} + \frac{2\mu}{\rho}\left(e_{ij}e_{ij} - \frac{1}{3}\Delta^2\right) + \frac{1}{\rho}\nabla.(k\nabla T) \tag{3}$$

where $e_{ij} = \frac{1}{2}\left(\frac{\partial u_i}{\partial x_j} + \frac{\partial u_j}{\partial x_i}\right)$ and $\Delta = e_{ii}$ (Batchelor, 1976).

2.4 Soot formation model

The detailed chemistry of soot formation is quite complicated, so it is only approximated in the models used by FLUENT. The transport equation for soot mass fraction can be written as,

$$\frac{\partial}{\partial t}(\rho Y_{soot}) + \nabla \cdot (\rho \vec{v} Y_{soot}) = \nabla \cdot \left(\frac{\mu_t}{\sigma_{soot}} \nabla Y_{soot}\right) + R_{soot} \tag{4}$$

Y_{soot} is the soot mass fraction, σ_{soot} is the turbulent Prandtl number for soot transport, and R_{soot} is the soot generation rate (kg/m^3-s).

The net rate of soot generation, R_{soot} is the difference of soot formation, R_{soot_form} and soot combustion, R_{soot_comb} given by,

$$R_{soot} = R_{soot\_form} - R_{soot\_comb} \tag{5}$$

The soot formation rate is given by empirical rate expression,

$$R_{soot\_form} = C_s p_{fuel} \emptyset^r e^{\frac{-E}{RT}} \tag{6}$$

where, C_s = soot formation constant (kg/N-m-s)

p_{fuel} = fuel partial pressure (Pa)

$\emptyset$ = equivalence ratio

r = equivalence ratio exponent

E/R = activation temperature (K)

The rate of soot combustion (Khan and Greeves, 1974; Magnussen and Hjertager, 1977) is given by the minimal of two rate expressions, R_1 and R_2, which are expressed as,

$$R_1 = A\rho Y_{soot}\frac{\varepsilon}{k} \tag{7}$$

$$R_2 = A\rho\left(\frac{Y_{ox}}{v_{soot}}\right)\left(\frac{Y_{soot}v_{soot}}{Y_{soot}v_{soot} + Y_{fuel}v_{fuel}}\right)\frac{\varepsilon}{k} \tag{8}$$

where A = constant in the Magnussen model

Y_{ox}, Y_{fuel} = mass fractions of oxidizer and fuel

v_{soot}, v_{fuel} = mass stoichiometries for soot and fuel combustion

Thus,

$$R_{soot\_comb} = \min\left[R_1\ ,\quad R_2\right] \tag{9}$$

The CFD package solves this set of transport equations for given boundary conditions by employing numerical methods such as Green-Gauss or least square method and predicts fluid flow dynamics and pressure, velocity, temperature, and concentration fields for different designs (Singh *et al.*, 2014).

3. Description of an experimental setup

The physical system consisted of the same diffusion flame setup that Singh *et al.* (2012) and Bharj *et al.* (2014) produced CNSs. The schematic view of the experimental setup is shown in fig. 1. It comprised a co-flow burner, substrate plate, traverse mechanism, oxygen, and fuel cylinders, rotameters, valves, acrylic sheet, and hose pipes. The burner consisted of two coaxially arranged concentric tubes of 10 mm and 50 mm, respectively, and 200 mm. The fuel was made to enter through a cylindrical duct having a diameter of 10 mm and oxygen through that having a diameter of 50 mm. The soot was collected on a stainless steel plate of dimensions 203×203 mm Grade 316 L. The operating conditions employed by Singh *et al.* (2012) and Bharj *et al.* (2014) during their experiments are given in tables 1 and 2, respectively.

4. CFD analysis

4.1 Geometry of computational domain

For numerical investigation, a 2D computational domain, 2000 mm in length and 400 mm in width, was chosen above the burner exit. The geometry of the domain was drawn with the exact dimensions as the actual experimental setup and is shown in fig. 2. Mesh was created using ANSYS meshing, and a grid independence test was performed, taking temperature variation along the axial direction as grid sensitivity parameter.

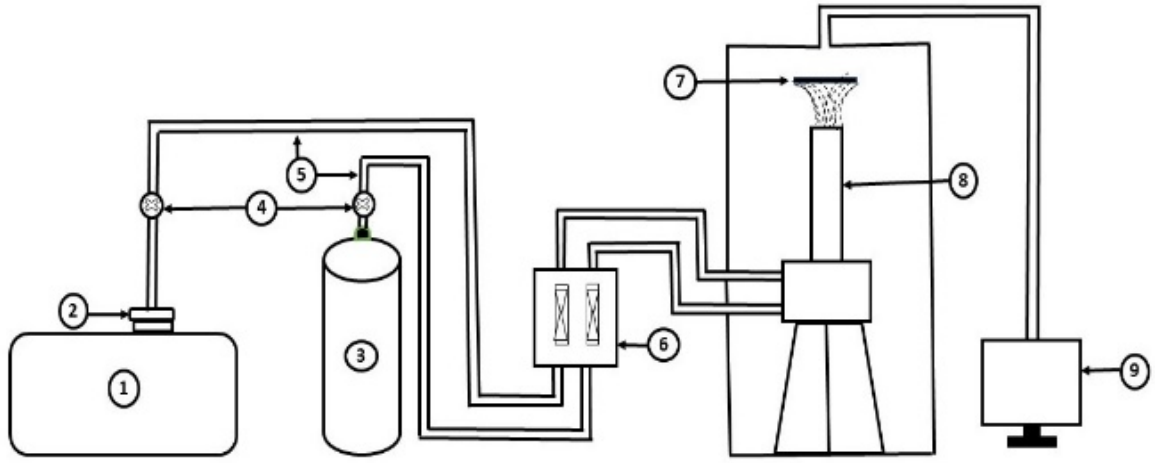

Fig. 1. Schematic view of the experimental setup: 1. Fuel tank 2. Safety valve 3. Oxygen cylinder 4. Flow control valves 5. Hose pipes 6. Rotameters 7. Substrate 8. Co-flow burner 9. Thermocouple readout

Table 1. Operating conditions for biogas – O_2 combustion

S. No.	Biogas flow rate, Q_B (lpm)	Oxygen flow rate, Q_{O2} (lpm)
1.	1	1
2.	1	2

Table 2. Operating conditions for LPG – O_2 combustion

S. No.	LPG flow rate, Q_L (lpm)	Oxygen flow rate, Q_{O2} (lpm)
1.	0.6	5.4
2.	0.6	15.6

4.2 Operating and boundary conditions

In ANSYS Fluent, the fuel and oxygen entry surfaces were specified as velocity inlets and outlet as pressure outlet. The solver employed was pressure-based with double precision. Following assumptions were made for numerical simulations: steady-state, no gas radiation, no surface reactions, and the outer wall were assumed to be adiabatic with the no-slip condition. A steady-state model that incorporates equations for conservation of mass, momentum, energy, and species was implemented to calculate the temperature and concentration distribution inside the flame. The standard k-ε model was employed for turbulence modeling and the non-premixed combustion model for reaction modeling. A PDF table was generated using biogas and LPG as fuels. The mole fraction ratio of CH_4: CO_2 in biogas and C_3H_8: C_4H_{10} in LPG were taken to be 0.77: 0.23 and 0.6: 0.4 respectively (as mentioned in the existing experimental data (Singh et al., 2012) and (Bharj et al., 2014)). The effect of radiation was ignored to shrink the computational cost. The Semi-Implicit Method for Pressure-Linked Equations (SIMPLE) algorithm with second-order upwind spatial discretization was used for pressure-velocity coupling. Convergence criteria for continuity, momentum, energy, and species are a value of residual less than 10^{-6}. The simulation allowed the estimation of temperature distribution and distribution of CO and soot mass fractions inside the flame at different flow rates (Pinho *et al.*, 2005; Silva *et al.*, 2007).

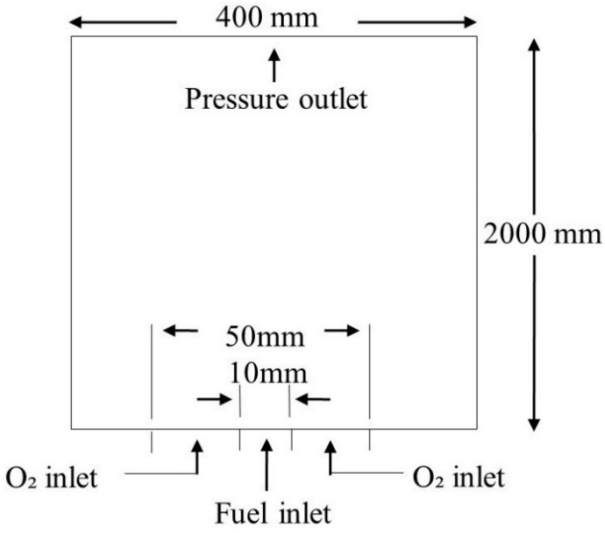

Fig. 2. Computational domain

5. Results and discussion

This investigation aims to analyze the soot formation in LPG and Biogas fueled diffusion flames. To understand the phenomenon more clearly, the flow structure inside the combustion chamber has been considered. Figure 3 presents the velocity streamlines inside the chamber at $Q_B = 1$ lpm and $Q_{O2} = 2$ lpm. In all cases, the flow pattern is similar, characterized by the upward flow of fuel and oxidizer species followed by their mixing through the diffusion process. The

velocity of the fluid is found to be maximum near the core of the chamber. The fuel and oxidizer flow fields substantially affect the species and temperature distribution inside the flame.

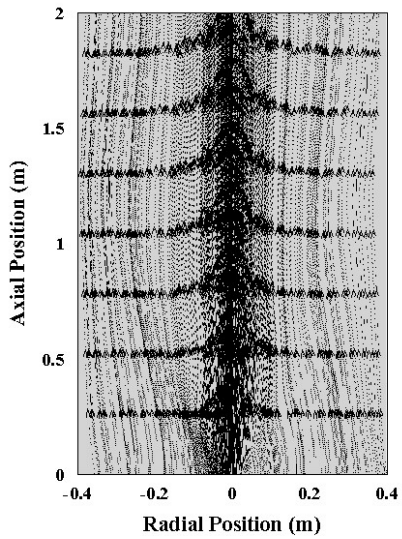

Fig. 3. Velocity streamlines in the chamber

Figures 4 and 5 show the temperature distribution inside the flame for biogas and LPG fuels, respectively. The peak flame temperature is higher with LPG fuel than with biogas due to the higher heating value of LPG. Also, it decreases with a decrease in the fuel to oxidizer velocity ratio. This is because intense heat is released at a low oxidizer flow rate due to the appreciable mixing of fuel and oxygen jets. The flame length is also higher at a lower flow rate of oxygen. More flame height results in more residence time for the flame to produce soot, leading to more production of CNSs (Patel and Shah, 2017).

The mass fraction variation of CO for biogas and LPG is depicted in figs. 6 and 7, respectively. LPG is associated with more CO formation as compared to biogas. Figures 8 and 9 show the variation of mass fraction of soot inside the flame for two fuels. As observed, the soot formed with LPG is significantly higher than with biogas. The ultimate release of CO and soot is thus determined by both flame chemistry and flow environment. Biogas being an organic fuel, releases less CO and soot than LPG.

Moreover, the peak soot mass fraction increases with the fuel to oxidizer velocity ratio. This is due to increased flame temperature and CO mass fraction with decreased oxidizer velocity. The high flame temperature facilitates the soot formation process by enhancing the pyrolysis reactions, leading to soot precursors' formation (Wey *et al.*, 1984; Naegeli *et al.*, 1983). Moreover, higher fuel to oxidizer velocity ratio gives rise to increased residence time from nucleation to the oxidation stage, permitting more growth of soot and hence CNS particles (Kaplan and Kailasanath, 2001). These results agree well with the experimental results of Singh *et al.* (2012) and Bharj *et al.* (2014), thereby validating the models being employed.

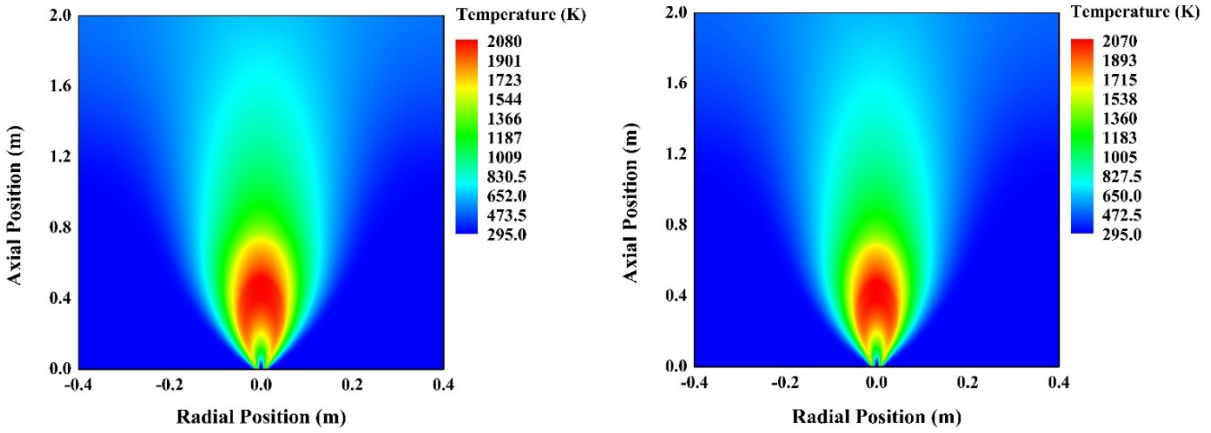

(i) (ii)

Fig. 4. Temperature contours at fixed biogas flow rate, 1 lpm (i) Q_{O2} = 1 lpm, (ii) Q_{O2} = 2 lpm

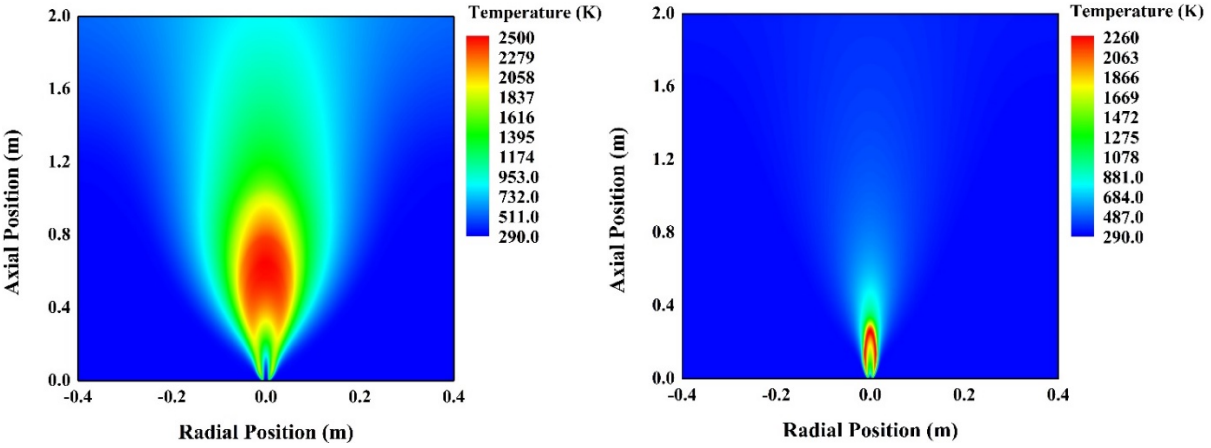

(i) (ii)

Fig. 5. Temperature contours at fixed LPG flow rate, 0.6 lpm (i) Q_{O2} = 5.4 lpm, (ii) Q_{O2} = 15.6 lpm

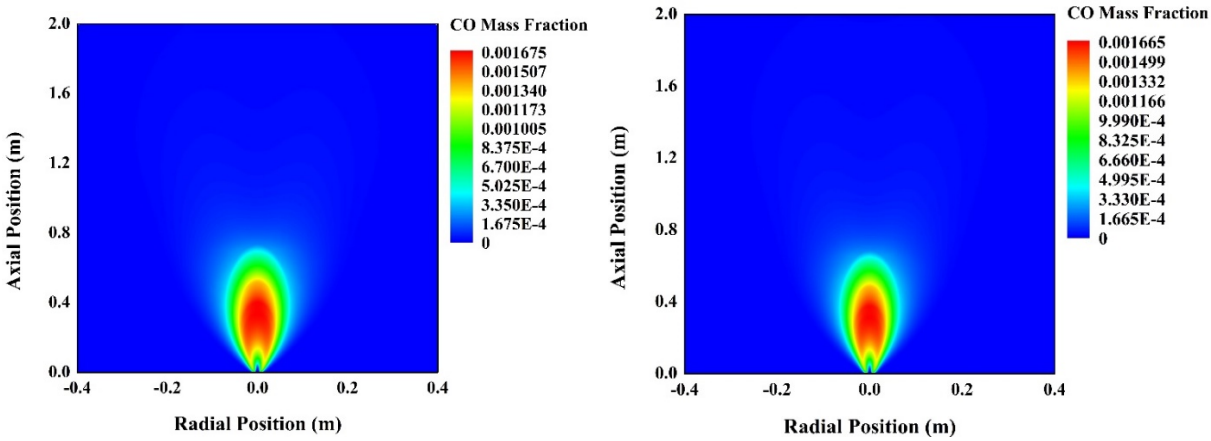

(i) (ii)

Fig. 6. Mass fraction variation of CO at fixed biogas flow rate, 1 lpm (i) Q_{O2} = 1 lpm, (ii) Q_{O2} = 2 lpm

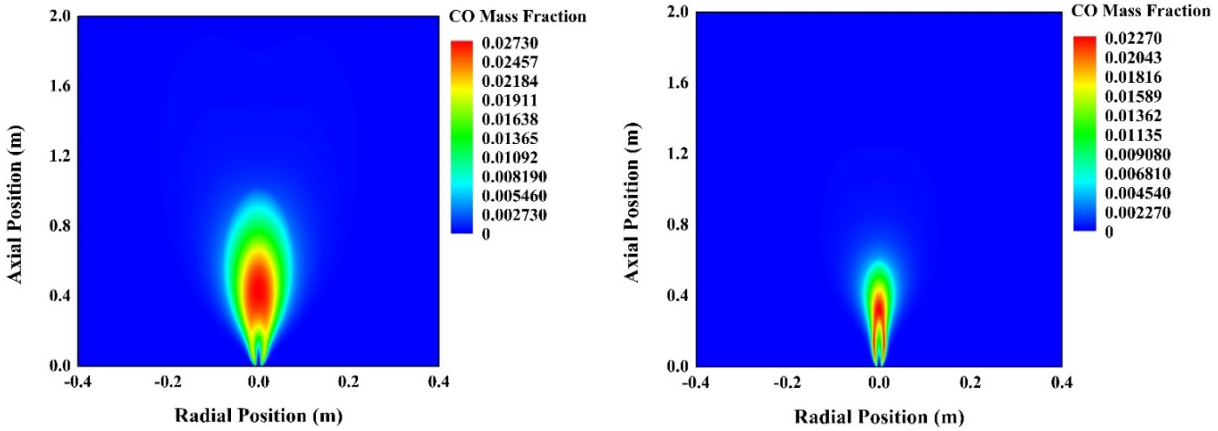

(i) (ii)

Fig. 7. Mass fraction variation of CO at fixed LPG flow rate, 0.6 lpm (i) Q_{O2} = 5.4 lpm, (ii) Q_{O2} = 15.6 lpm

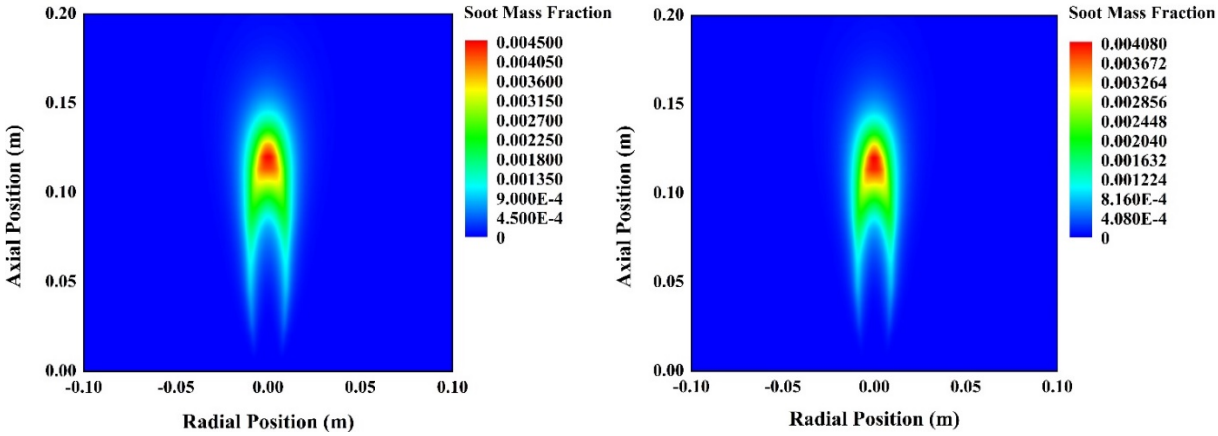

(i) (ii)

Fig. 8. Mass fraction variation of soot at fixed biogas flow rate, 1 lpm (i) Q_{O2} = 1 lpm, (ii) Q_{O2} = 2 lpm

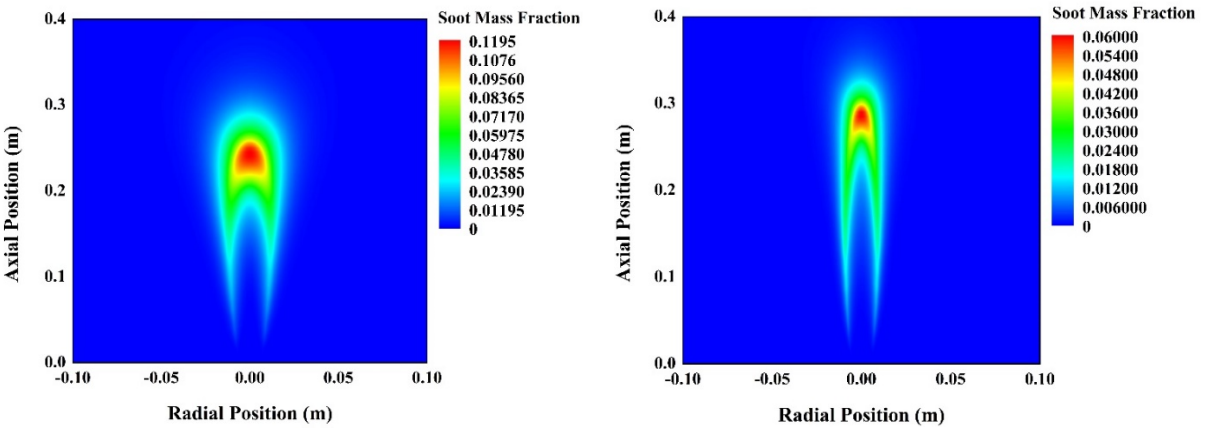

(i) (ii)

Fig. 9. Mass fraction variation of soot at fixed LPG flow rate, 0.6 lpm (i) Q_{O2} = 5.4 lpm, (ii) Q_{O2} = 15.6 lpm

The temperature variation along the axis of the burner with both fuels is shown in fig. 10. It can be observed that the temperature at the exit of the burner is the same as atmospheric temperature. As we move away from the burner exit, the axial temperature increases rapidly due to heat diffusion towards the axis. The temperature increases at a certain axial distance and decreases due to radially outward heat diffusion. Figure 11 shows the radial temperature distribution for both flames at a flame height of 45 mm above the burner exit. As we move radially away from the outer wall of the combustion chamber towards the axis, the temperature remains constant within a particular region. Then it starts increasing and reaches the maximum value. At this point, a non-premixed flame is produced. Afterward, the temperature is reduced from the peak towards the axis of the combustion chamber because fuel flowing in the middle stream absorbs the heat. Figures 12 and 13 depict the axial and radial variation of soot mass fraction at a flame height of 45 mm, respectively. The soot mass fraction pursues the same trend as temperature variation. The soot formed is maximum at nearly 1200 K for biogas and 1600 K for LPG. We can locate the axial and radial positions at which full soot will be obtained from these graphs. The function of that point is different for both fuels due to different flame environments in each case.

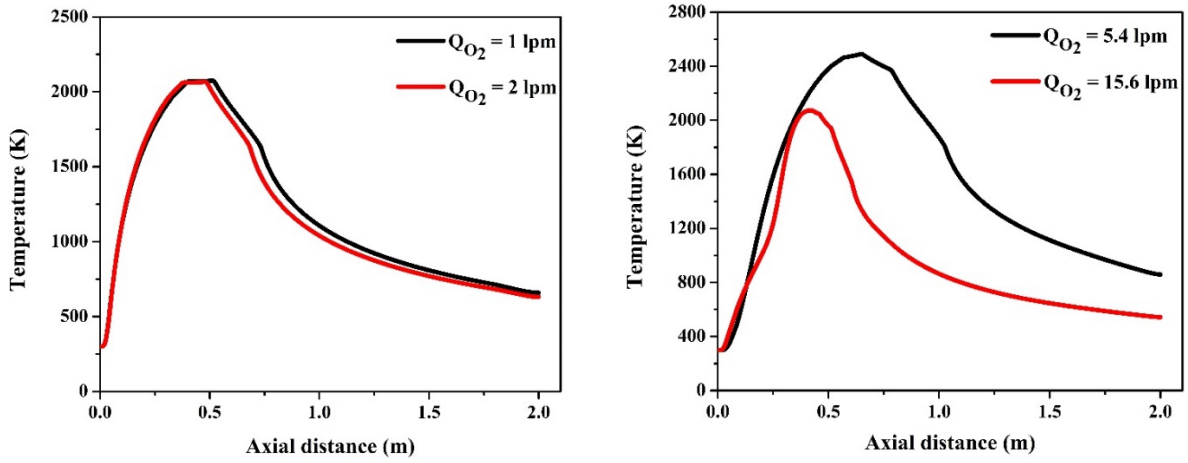

(i) (ii)

Fig. 10. Axial temperature variation (i) at a fixed biogas flow rate (1 lpm), (ii) at fixed LPG flow rate (0.6 lpm)

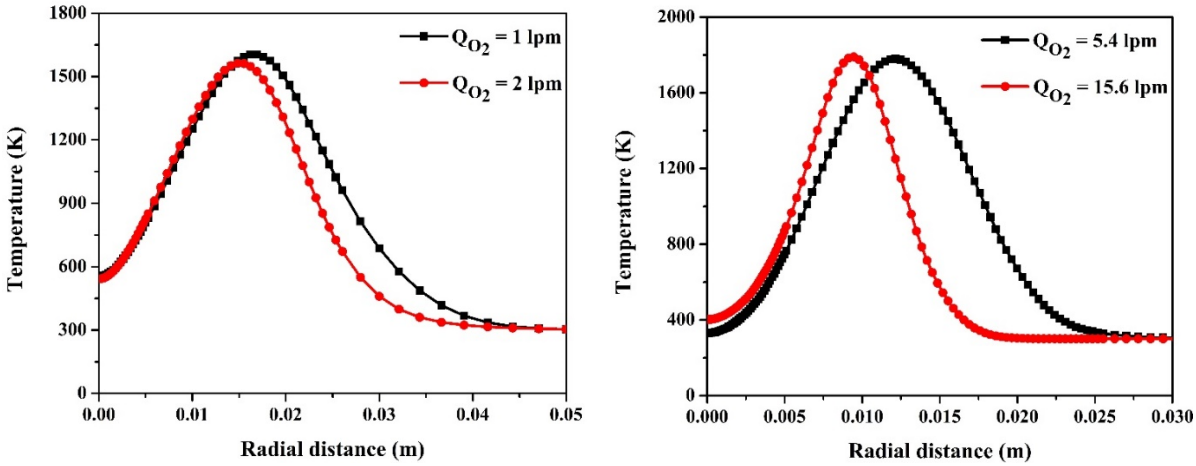

(i) (ii)

Fig. 11. Radial temperature distribution at a flame height of 45 mm (i) for fixed biogas flow rate (1 lpm), (ii) for fixed LPG flow rate (0.6 lpm)

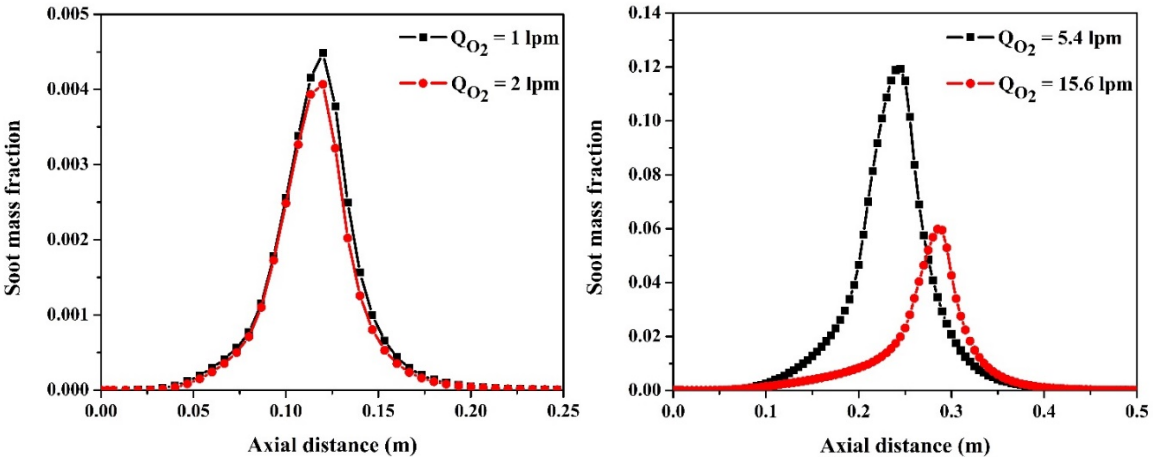

(i) (ii)

Fig. 12. Axial variation of soot mass fraction (i) for fixed biogas flow rate (1 lpm), (ii) for fixed LPG flow rate (0.6 lpm)

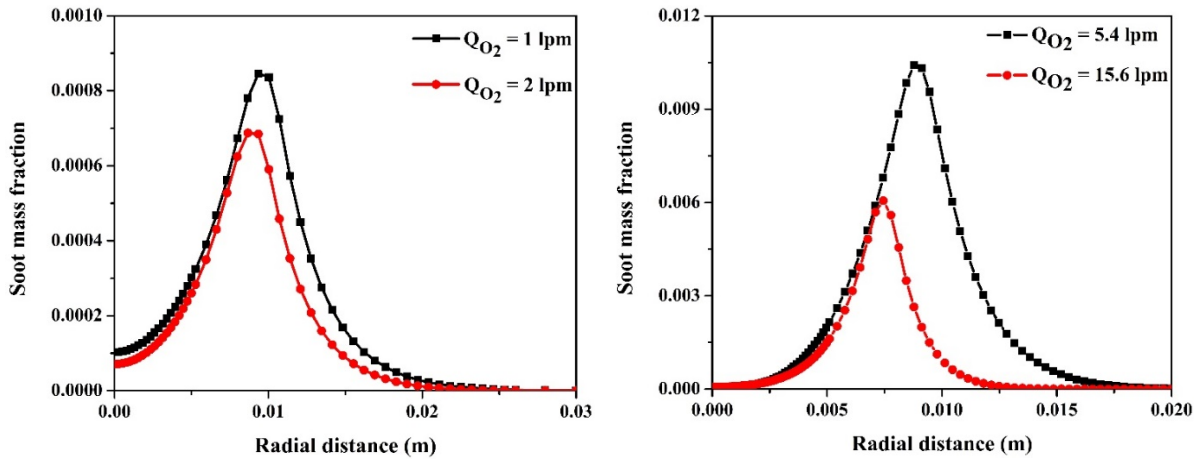

(i) (ii)

Fig. 13. Radial distribution of soot mass fraction at a flame height of 45 mm (i) for fixed biogas flow rate (1 lpm), (ii) for fixed LPG flow rate (0.6 lpm)

From the above results, it can be seen that different types of fuels provide a different chemical environment conducive to the growth of CNSs. The fuel and oxidizer mainly govern the diffusion flame's gas-phase composition and temperature. Furthermore, the reactions in various flame regions can also be depicted from temperature and species concentration in that region. Pyrolysis reactions occur near the bottom of the flame in the high-temperature region. These reactions lead to the formation of CO_2, CO, and other partial oxidation products along with secondary hydrocarbon species, radicals, *etc.* (Gore and Sane, 2011). The mixture of these intermediate precursors initiates the nucleation process of CNSs. Afterward, the surface growth of particles takes place in a nearby region. The top region of the flame is characterized as the oxidation region, where the formed solid phase material undergoes oxidation reactions, thus

giving minimum yield at that location. The schematic of each process is depicted in fig. 14. This study can further help in future research in optimizing combustion equipment and flame parameters so that maximum yield of CNSs can be obtained.

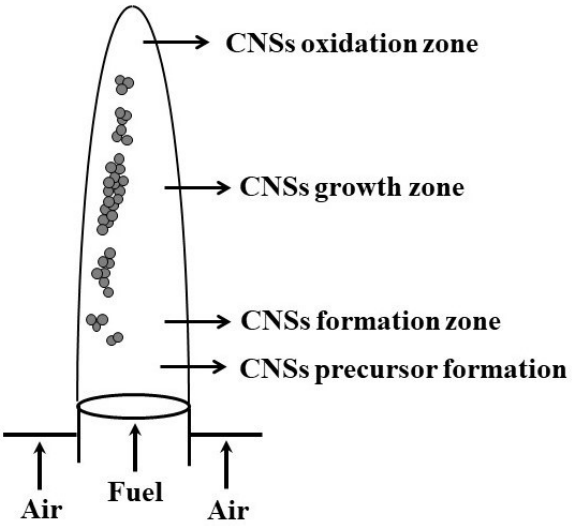

Fig. 14. Schematic of CNSs formation in a diffusion flame

6. Conclusion

Direct numerical simulation has been conducted on non-premixed combustion of biogas and LPG fuels. The formation of CNSs using these fuels has already been observed in the experiments of Bharj *et al*. However, the numerical modeling allows a deep understanding of their formation mechanism within the flame. The fluid dynamics of the diffusion flame are obtained by solving Navier-Stokes equations. The energy and species equations and continuity and momentum equations are solved to specify mass and energy transfer. The distribution of temperature and mass fractions of CO and soot inside the flame is plotted for both fuels. The growth rate of soot and CNSs depends explicitly on the type of fuel used and flow rates of fuel and oxidizer. The formation is hastened by the elevated flame temperature and high precursor concentrations that are inducive to their growth. The numerical simulation also helps interpret various reactions in different regions of the flame. The bottom area of flame is dominated by the pyrolysis reactions of fuel molecules, which lead to the formation of intermediate precursors. These precursors further initiate the nucleation of carbon nanostructures in the nearby region, followed by their surface growth and oxidation near the top areas. A detailed understanding of phenomena using simulation tools can help predict optimal conditions for product formation for future research.

ACKNOWLEDGMENTS

The authors are grateful to Director Dr. B. R. Ambedkar, National Institute of Technology, Jalandhar, for providing the necessary administrative and financial support in conducting the present study.

References

Batchelor, GK (1967). An Introduction to Fluid Dynamics. Cambridge University Press, England.

Bharj, J., Singh, S., Chander, S. & Singh, R. (2014). Biogas: a natural and renewable source for carbon nanotubes. International Journal of Research in Advent Technology, **2**(3): 54-59.

Busupally, M. R. & De, A. (2016). Numerical modeling of soot formation in a turbulent C2H4/air diffusion flame. International Journal of Spray and Combustion Dynamics, **8**(2): 67-85.

Choudhary, R., Kale, M. & Dixit, S. K. (2015). A computational evaluation of emissions for non-premixed natural gas combustion. International Journal of Scientific Research Engineering and Technology, **4**: 731-735.

Gore & Sane, A. (2011). Flame Synthesis of Carbon Nanotubes. In: Yellampalli, S. (Ed.) Carbon Nanotubes - Synthesis, Characterization, and Applications. Rijeka, Intech Open.

Kaplan, C. & Kailasanath, K. (2001). Flow-field effects on soot formation in normal and inverse methane-air diffusion flames. Combustion and Flame, **124**(1): 275-294.

Khan, I. M. & Greeves, G. (1974). A Method for Calculating the Formation and Combustion of Soot in Diesel Engines. In: Afgan, NH. & Beer, JM (Eds.) Heat Transfer in Flames. Washington DC, Scripta.

Kurzepa, L., Bulmer, J., Raus, A.L., Patmore, J. & Koziol K. (2014). Electrical properties of carbon nanotube-based fibers and their future use in electrical wiring. Advanced Functional Materials, **24**: 3661-3682.

Magnussen, B. F. & Hjertager, B. H. (1977). On mathematical models of turbulent combustion with particular emphasis on soot formation and combustion. Symposium (International) on Combustion, **16**: 719.

Mahdavian, L. (2017). Simulation and calculation of 2, 4, 5, 2′, 4′, 5′ -hexachlorobiphenyl passing from the central axis of single-walled carbon nanotube. Kuwait Journal of Science, **44**(2): 97-104.

Naegeli, D. W., Dodge, L. G. & Moses, C. A. (1983). Effects of flame temperature and fuel composition on soot formation in gas turbine combustors. Combustion Science and Technology, **35**: 117-131.

Noor, M., Wandel, A. & Yusaf, T. (2013). Detail guide for CFD on the simulation of biogas combustion in bluff body mild burner. Proceedings of the International Conference on Mechanical Engineering Research (ICMER), Malaysia.

Patel, V. & Shah, R. (2017). Experimental and numerical investigation of LPG fuelled inverse diffusion flame in a coaxial burner. International Journal of Advanced Thermofluid Research, **3**(1): 16-29.

Pinho, C.E.L., Delgado, J.M.P.Q., Pilao, R., Conde, J. & Pinho, C. (2005). Numerical study of propane-air mixture combustion in a burner element. Defect and Diffusion Forum, **273:** 144-149.

Shirneshan, A. & Jamalvand, H. (2016). Numerical investigation of combustion of biomass, methane, and gasoline fuels and emissions from a furnace chamber. Energy Policy, **3**(1): 19-26.

Silva, C. V., Franca, F. H. R. & Vielmo, H. A. (2007). Analysis of the turbulent, non-premixed combustion of natural gas in a cylindrical chamber with and without thermal radiation. Combustion Science and Technology, **179**(8): 1605-1630.

Singh, K. D., Gangadharan, P., Chen, D.H., Lou, H.H., Li, X. *et al.* (2014). Computational fluid dynamics modeling of laboratory flames and an industrial flare. Journal of Air and Waste Management Association, **64**(11): 1328-1340.

Singh, R., Deep, A., Bharj, J. & Nishtha, A. (2012). Optimization of flame synthesis of CNT structures using statistical experiments (SDOE). Bulletin of Electrical Engineering and Informatics, **1**(4): 305-312.

Smooke, M.D., Long, M.B., Connelly, B.C., Colket, M.B. & Hall, R.J. (2005). Soot formation in laminar diffusion flames. Combustion and Flame, **143**(4): 613-628.

Vander Wal, R., Ticich, T. & Curtis, V. (2000). Diffusion flame synthesis of single-walled carbon nanotubes. Chemical Physics Letters, **323**(3): 217-223.

Wang, Y., Wei, H., Lu, Y., Wei, S., Wujcik, E.K., *et al.* (2015). Multifunctional carbon nanostructures for advanced energy storage applications. Nanomaterials, **5:** 755-777.

Wey, C., Powell, E. A. & Jagoda, J. I.. (1984). The effect of temperature on the sooting behavior of laminar diffusion flames. Combustion Science and Technology, **41:** 173-190.

Yuan, L., Li, T. & Saito, K. (2003). Growth mechanism of carbon nanotubes in methane diffusion flames. Carbon, **41**(10): 1889-1896.

Zohra, K. F., Mounir, A. & Salah, C. (2017). Numerical simulation of CH4-H2-air non-premixed flame stabilized by a bluff body. Energy Procedia, **139:** 530-536.

Submitted: 12/01/2021
Revised: 16/04/2021
Accepted: 26/12/2021
DOI: 10.48129/kjs.11637